NASA Technical Memorandum 103867

45748

P. 11

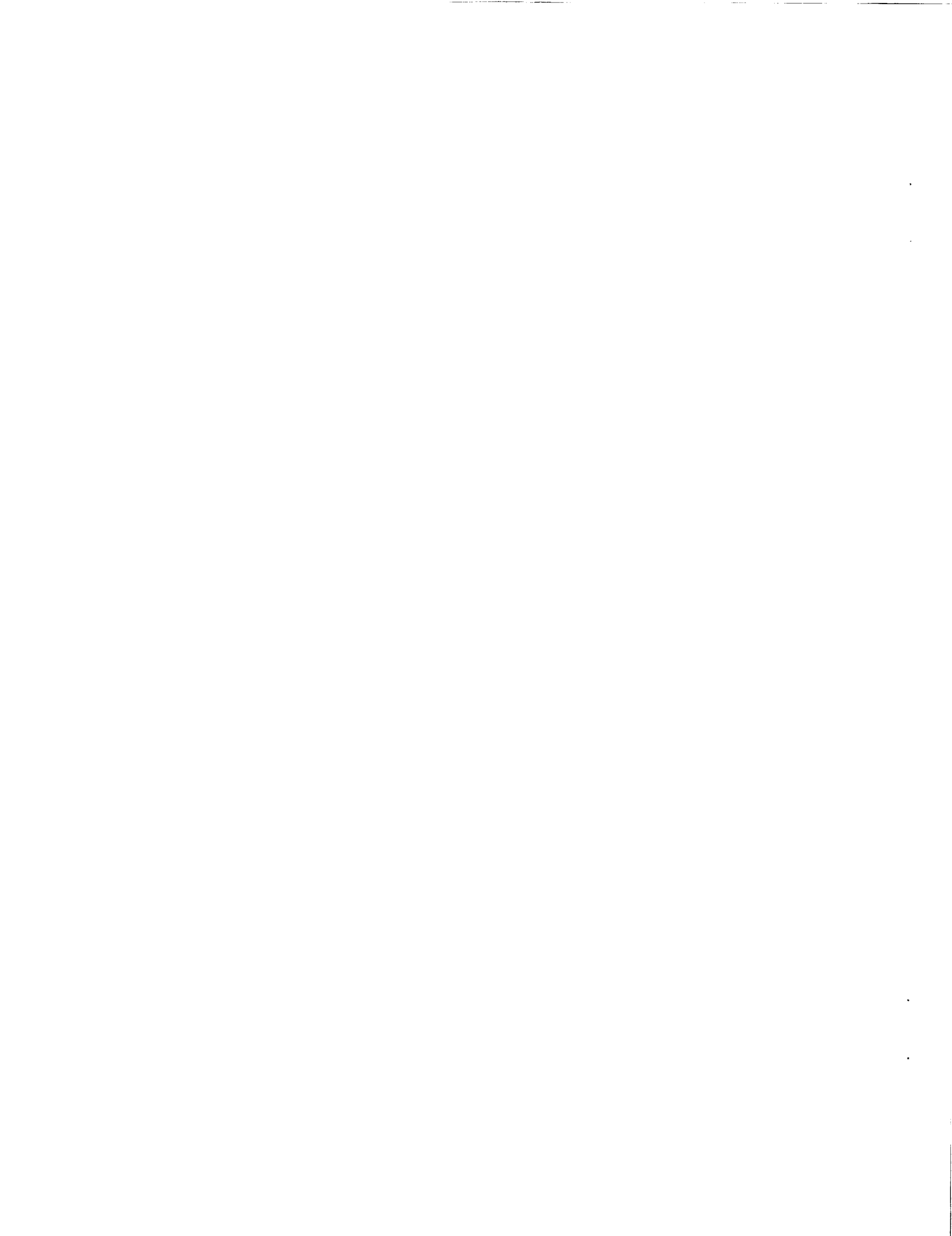# Aeroelastic Loads and Stability Investigation of a Full-Scale Hingeless Rotor

Randall L. Peterson, Ames Research Center, Moffett Field, California
Wayne Johnson, Johnson Aeronautics, Palo Alto, California

July 1991

NASA

National Aeronautics and
Space Administration

Ames Research Center
Moffett Field, California 94035-1000

Aeroelastic Loads and Stability Investigation of a Full-Scale Hingeless Rotor

Randall L. Peterson and Wayne Johnson

July 1991

NASA

National Aeronautics and
Space Administration

AEROELASTIC LOADS AND STABILITY INVESTIGATION OF A FULL-SCALE HINGELESS ROTOR

Randall L. Peterson

NASA Ames Research Center

Moffett Field, CA

Wayne Johnson

Johnson Aeronautics

Palo Alto, CA

ABSTRACT

An analytical investigation was conducted to study the influence of various parameters on predicting the aeroelastic loads and stability of a full-scale hingeless rotor in hover and forward flight. The CAMRAD/JA (for Comprehensive Analytical Model of Rotorcraft Aerodynamics and Dynamics, Johnson Aeronautics) analysis code is used to obtain the analytical predictions. Data are presented for rotor blade bending and torsional moments as well as inplane damping data obtained for rotor operation in hover at a constant rotor rotational speed of 425 rpm and thrust coefficients between 0.0 and 0.12. Experimental data presented are from a test in the NASA Ames 40- by 80-Foot Wind Tunnel. Validation of the rotor system structural model with experimental rotor blade loads data shows excellent correlation with analytical results. Using this analysis, the influence of different aerodynamic inflow models, the number of generalized blade and body degrees of freedom, and the control-system stiffness at predicted stability levels are shown. Forward flight predictions of the BO-105 rotor system on the Ames Rotor Test Apparatus for 1-g thrust conditions at advance ratios of 0.0 to 0.35 are presented. The influence of different aerodynamic inflow models, dynamic inflow models and shaft angle variations on predicted stability levels are shown as a function of advance ratio.

NOMENCLATURE

c	blade chord, ft
C_P/σ	rotor power coefficient, rotor power/$\rho S(\Omega R)^3$
C_T/σ	rotor thrust coefficient, shaft axes, thrust/$\rho S(\Omega R)^2$
I_θ	rigid-blade pitch inertia about feathering axis, slug-ft^2
K_θ	rotor cyclic control-system stiffness, ft-lb/rad
R	rotor radius, ft
S	rotor reference area, 4cR, ft^2
V	velocity, ft/sec
α_s	rotor shaft angle, positive shaft tilt aft, deg
μ	advance ratio, $V/\Omega R$
ρ	air density, slug/ft^3
σ	damping decay coefficient, sec^{-1}; or rotor solidity
ω_ζ	rotor-blade fundamental inplane bending frequency, rad/sec
ω_θ	nonrotating cyclic control-system frequency, per rev at design tip speed
Ω	rotor rotation frequency, rad/sec

INTRODUCTION

Proposed advances in rotor-hub design hold promise for major improvements in rotorcraft performance. Reducing the complexity of and the number of parts in the rotor-hub system will improve hub aerodynamics, increase reliability, and reduce maintenance requirements. Additionally, hingeless and bearingless hubs provide increased control power over that of conventional articulated rotor systems. Improved hingeless and bearingless rotors with advanced hub designs are being pursued to improve the capability and reliability of future helicopters. The design of these advanced rotor-hub systems will require validated analytical codes that can reliably predict rotor performance, loads and stability. Many experimental studies have been made in which the emphasis was on evaluating the aeromechanical stability of advanced rotor-hub systems. In most of that work, however, model-scale rotor systems were used. As a result, there are still questions about geometric, dynamic, and aerodynamic scaling and fabrication details, and a need exists for accurately defining the operational characteristics of full-scale advanced helicopter rotor systems. Once the necessary data are obtained, they can be used to validate theoretical prediction codes and to identify areas where current analytical techniques must be further developed.

This paper presents results from a 1983 hover test of a BO-105 helicopter rotor system in the NASA Ames Research Center 40- by 80-Foot Wind Tunnel test section (Fig. 1). Rotor performance, loads and inplane damping were obtained for rotor operation between 350 and 425 rpm (design speed) and for rotor thrust coefficients (C_T/σ) between 0.0 and 0.12. Data in this paper are presented for rotor operation at 425 rpm and thrust coefficients from 0.0 to 0.12. Additional data pertaining to this test can be found in Ref. 1. The test results are considered an important addition to the relatively few, well-documented aeroelastic stability data sets that currently exist for full-scale hingeless rotor systems.

To demonstrate the usefulness of this data set, correlation with a comprehensive rotorcraft dynamics analysis code is performed.[2]

1

Correlation with the 1983 hover test data was previously performed.[3,4] The results reported in this paper used an improved structural model that is validated using rotor blade bending and torsional moment data acquired in the above test program. Using this code, the influences of varying the number of generalized blade and body degrees of freedom, and of the control-system stiffness on predicted stability levels are studied. As reported by various other researchers, the use of an unsteady aerodynamic model (dynamic inflow) can at times significantly improve correlation with experimental results. The use of an analytical model without dynamic inflow, with a quasi-static inflow model, and with a dynamic inflow model are compared in this paper with the experimental data. Forward flight stability predictions at a constant 1-g rotor thrust condition as a function of advance ratio for both a trimmed propulsive force condition and constant rotor shaft angle are presented.

TEST HARDWARE

The BO-105 helicopter rotor system is a four-bladed, soft inplane ($\omega_\zeta < \Omega$) hingeless rotor with constant chord (0.866 ft), −8° linear twist, and a NACA 23012 cambered airfoil. The rotor radius is 16.11 ft; solidity (σ) is 0.07. The rotor hub has 2.5° of built-in coning and zero droop or sweep of the blade outboard of the pitch bearing (Fig. 2). The BO-105 rotor used in this test was a production rotor set previously used in a flight-test program. Additional details about the rotor system are presented in Table 1 and in Ref. 5. Calculated rotating coupled bending and torsion frequencies at the design tip speed of 717 ft/sec (425 rpm) are presented in Table 2.

The rotor was installed on the Rotor Test Apparatus at Ames (Fig. 1). This apparatus is a special-purpose drive and support system for operating helicopter rotors in the 40- by 80-Foot Wind Tunnel. It houses two electric drive motors, the hydraulic servo-actuators of the primary control-system, and a dynamic control system capable of introducing dynamic perturbations to the non-rotating swashplate (collective and tilt) at frequencies up to 30 Hz. This system is used to excite the rotor at its fundamental inplane bending frequency for stability measurements.

PERFORMANCE TESTING

Hover testing of the BO-105 rotor system was performed with the wind-tunnel access doors open and with the rotor shaft tilted forward 10° to reduce airflow recirculation (Fig. 1). Test conditions were established by setting the rotor rotation speed and rotor thrust coefficient (C_T/σ). Cyclic pitch was used to nominally null any once-per-revolution flapping, as measured using a resolved flapwise bending moment signal near the blade root at station 0.10R. Both longitudinal and lateral cyclic pitch inputs of the order of ±0.2° were required to null this once-per-revolution flapping.

STABILITY TESTING

A transient decay time-history from an edgewise bending-moment signal (station 0.10R) was used to determine system stability. The damping level was determined for only the fundamental edgewise bending mode. After obtaining the desired operating conditions, the dynamic control-system was used to oscillate the cyclic pitch at the rotor regressing inplane bending frequency (nutation type excitation). A chordwise bending moment signal was monitored, and the amplitude of the swashplate oscillation was increased until either an adequate signal at

the forcing frequency was obtained in the blade chordwise bending moment, or a load limit was reached at any of the instrumented blade stations. Abrupt termination of the excitation yielded the transient decay of the blade edgewise bending moment signal. This signal was recorded and analyzed to determine inplane damping. For repeatability, several stability records were obtained at each operating condition.

As mentioned above, excitation of blade edgewise bending motion was accomplished by oscillating the swashplate at the regressing inplane modal frequency. Because of this control input, the rotor responded to blade-pitch motion at the regressing inplane modal frequency in the rotating system. The resulting transient decay record obtained from the edgewise bending-moment signal yielded the damping information for the regressing inplane mode. Since the progressing inplane mode was not excited, it should not contaminate the transient decay time-history data or the damping determination. This excitation technique is considered superior to either step or impulse inputs to the rotor control-system or body modes since it does not require time histories from each blade (and a subsequent multiblade coordinate transformation) to determine the rotor inplane modal characteristics. It should be noted that this means of rotor-mode excitation also could be used to excite the progressing inplane mode separately, although this was not done in this test. However, analytical results presented in Ref. 3 show that the experimental data are for the regressing inplane mode, which is typically the most important rotor mode for aeromechanical considerations such as ground or air resonance.

HOVER TEST RESULTS

Rotor Blade Loads Data

Experimentally measured steady edgewise, flapwise, and torsional moment data acquired at a rotor rotational speed of 425 rpm as a function of rotor thrust coefficient are shown in Figures 3-5. Steady edgewise blade bending moment data are shown in Figure 3 at an inboard radial station (r/R = 0.10) as measured on two different blades. The second blade had only one instrumented radial station (edgewise only) from which bending moment data were acquired. Figure 3 also presents edgewise bending moment data at a midspan radial station (r/R = 0.57). Steady flapwise bending moment data are shown in Figure 4. Flapwise bending moment data at both an inboard radial station (r/R = 0.10) and at a midspan radial station (r/R = 0.57) are shown. Steady torsional moment data as a function of rotor thrust coefficient are shown in Figure 5. Data are presented for an inboard radial station (r/R = 0.34).

Correlation of rotor blade bending and torsional moment data with analytical results[2] are shown in Figures 6-8. The definition of the rotor structural properties was provided to NASA and the U.S. Army by Messerschmitt-Bölkow-Blohm GmbH (MBB) and the Deutsche Forschungsanstalt für Luft-und Raumfahrt e.V. (DLR Institute for Flight Mechanics) under the auspices of the U.S. Army/German Memorandum of Understanding on Cooperative Research in the Field of Helicopter Aeromechanics. The key rotor blade cross-sectional structural modeling parameters are presented in Table 3. Ten bending (7 flapwise, 3 edgewise) and three torsion (1 rigid, 2 elastic) modes were modeled in the analysis for the results presented. The flapwise and edgewise stiffness values in the structural model for the hub region (r/R = 0.0 to 0.06) were adjusted to model accurately the fundamental flapwise and edgewise frequencies of 0.66/rev and 1.12/rev in the analysis (Table 2). These values are representative of those reported in Refs. 6 and 7.

Correlation of the experimentally acquired steady edgewise bending moment data with analytical results is presented in Figure 6. Correlation of steady edgewise bending moment data (Fig. 3) with analytical results at both an inboard radial station (r/R = 0.10) and from a midspan radial station (r/R = 0.57) is shown. For the inboard radial station, the trend with rotor thrust is well predicted, however, the analytical results are offset from the experimental data by approximately 6500 in-lbs at the design rotor thrust coefficient ($C_T/\sigma = 0.07$). For the midspan radial station, the trend with rotor thrust is also well predicted, however, the analytical results are offset from the experimental data by approximately 1000 in-lbs at the design rotor thrust coefficient.

To improve correlation of the edgewise bending moment data, various parameters, including the number of blade bending degrees of freedom and the chordwise location of the elastic axis, were varied. Using less than 10 bending (7 flapwise, 3 edgewise) modes did not improve the correlation for the edgewise bending, and instead had the effect of skewing both the flapwise and edgewise trends with rotor thrust. Minor variations in the location of the elastic axis relative to the blade leading edge had a significant impact on the predicted edgewise bending moments with little or no effect on either the flapwise or torsional moment results. Figure 7 presents the correlation of the experimentally acquired edgewise bending moment data with analytical results for an aft shift of the elastic axis location from 15.6% to the 17.95% chordwise location as referenced from the blade leading edge. The blade tension center, center of gravity, control axes and aerodynamic center locations remained fixed relative to the blade leading edge. For the inboard radial station, the offset of the analytical results from the experimental data has been reduced approximately 85% to less than 1000 in-lbs from that shown in Figure 6 at the design rotor thrust coefficient ($C_T/\sigma = 0.07$). For the midspan radial station, the offset has been reduced approximately 50% to less than 500 in-lbs from that shown in Figure 6 at the design rotor thrust coefficient. No significant changes in either the flapwise and torsional moment results were noted.

In the analysis, the blade is modeled with a coincident feathering axis and elastic axis (sweep of the elastic axis relative to the feathering axis can be introduced, but would not be appropriate for this rotor). The actual rotor has the feathering axis at 25% chord and the elastic axis at 15.6% chord. The control-system stiffness is about five times the blade torsional stiffness for the wind tunnel installation. The baseline calculations (Fig. 6) were performed with both the feathering axis and elastic axis at the 15.6% chord. The improved correlation with the axes both at 17.95% chord (Fig. 7) can be viewed as the result of a better model for the elastic axis in the wind tunnel configuration.

Correlation of the experimentally acquired steady flapwise bending moment data with analytical results are presented in Figure 8. Correlation of steady flapwise bending moment data (Fig. 4) with analytical results (with the baseline properties, Table 3) at both an inboard radial station (r/R = 0.10) and from a midspan radial station (r/R = 0.57) are shown. For the inboard radial station, the trend and magnitude with rotor thrust are well predicted, particularly at the design rotor thrust coefficient ($C_T/\sigma = 0.07$). For the midspan radial station, the trend and magnitude are well predicted over the entire thrust range.

Correlation of the experimentally acquired steady torsional moment data with analytical results at an inboard radial station (r/R = 0.34) are presented in Figure 9. The trend and magnitude with rotor thrust are well predicted over the entire thrust range.

The remaining analytical results presented are in support of the pretest predictions for the wind tunnel test of the BO-105 hinge-less rotor system. The results are calculated using the modified elastic axis location and ten bending and three torsion modes for the rotor trim solution.

Rotor Stability Data

Stability data for a rotor rotational speed of 425 rpm as a function of rotor thrust coefficient are shown in Figure 10. Each plotted point is for a unique data record. The results presented in Figure 10 differ from those presented in Refs. 3 and 4, in that previously the Moving-Block[8] data reduction technique was used to estimate damping from the transient decay data. The technique used in this study is based on the least-squares method developed by Wilcox and Crawford[9] for reduction of free-oscillation data acquired in a wind tunnel test. This technique was adapted to analyze multiple-mode transient decay records for rotor-stability testing. Comparisons of this technique using analytical data with the widely used Moving Block technique have shown it to be superior in analyzing transient decays containing moderate to significant levels of periodic forced response from the rotor. This technique is also superior in analyzing transient decays containing modes closely spaced in frequency and high levels of damping.

Scatter in the experimentally determined decay coefficients is small at the lower damping levels. Damping is greatest at high rotor thrust and reduces with rotor thrust. The levels of damping data scatter from this experiment compare with good quality stability data obtained in several other experiments. When the system is lightly damped, good quality transient decay records can be obtained, and the resulting measured damping values are very repeatable. For several reasons, increased scatter is obtained at highly damped conditions; for example, difficulty in exciting the regressing lag mode (due to blade structural load limitations), a short duration transient, or a poor single or multiple-degree of freedom decay curve-fit. Given the inherent limitations of the test procedures and the resulting data-scatter bands, the important trends are evident despite what may appear to be significant data scatter at high thrust operating conditions.

Correlation of stability data with analytical prediction[2] are shown in Figures 11-13. Since a four-bladed rotor was used in the hover operating condition and measurements are for the regressing lag mode, only cyclic rotor modes for elastic-blade bending and rigid and elastic blade torsion deflections were modeled in the aeroelastic stability analysis. The collective and reactionless rotor modes were not modeled, a result of the lack of coupling with other rotor and support modes. A blade structural damping level of 3% critical is used for results presented in Figures 11-13. This value is an increase over that used in Refs. 3 and 4 by a factor of two. A value of 3% is representative of the values used in Refs. 6, 7, and 10. A value of 1.5% resulted in a uniform decrease of the predicted decay coefficients with no change in the trends with thrust in this study and in Refs. 3 and 4. As discussed in detail in Ref. 3, two support-system degrees of freedom, the first-balance longitudinal mode and the first-balance lateral mode, were modeled in the analysis. Using from zero to six support degrees of freedom in the analysis did not significantly influence the predicted decay coefficients of the inplane modes. Therefore the results presented here represent isolated rotor stability.

The influence of varying the number of rotor modes in the aeroelastic stability analysis of Ref. 2 is shown in Figure 11 for a rotor rotational speed of 425 rpm. The open symbols represent

the experimental data shown in Figure 10. A baseline cyclic rotor control-system stiffness yielding a nonrotating $\omega_\theta = 7.3$ per rev rigid torsion modal frequency was used. A dynamic inflow model was used in the stability analysis for the results presented in Figure 11. Results for different numbers of bending and torsion rotor modes are shown. When only rotor bending is modeled (fundamental flap and lead-lag modes), damping is overpredicted for $C_T/\sigma < 0.07$ and underpredicted for $C_T/\sigma > 0.07$. Introducing a rigid cyclic torsion mode reduces damping for $C_T/\sigma \leq 0.09$. Including the first elastic torsion mode reduces the regressing inplane modal damping significantly over the entire thrust range shown. The torsion modes introduce effective pitch-lag coupling, which has a significant influence on stability, as discussed in Ref. 7. Additionally modeling the second flap and lead-lag cyclic bending modes is shown to have little influence on the predicted results.

The influence of different aerodynamic models is shown in Figure 12. Results are shown for a rotor rotational speed of 425 rpm with a static aerodynamic inflow model, a quasi-static inflow model, and a dynamic inflow model. A baseline cyclic control-system nonrotating frequency of $\omega_\theta = 7.3$ per rev was modeled. The static inflow model underpredicts damping for $C_T/\sigma > 0.02$. The dynamic inflow model predicts damping well at low thrust conditions ($C_T/\sigma \leq 0.04$), and like the static inflow model it underpredicts damping at moderate to high thrust conditions ($C_T/\sigma > 0.04$). The quasi-static model overpredicts damping at low thrust conditions ($C_T/\sigma < 0.05$) and underpredicts damping at moderate to high thrust conditions similar to both the static and dynamic inflow models. The quasi-static inflow model is the least sensitive to thrust variations of the three aerodynamic models. The static inflow model is the most sensitive to thrust variations and gives the best agreement with experimental data at $C_T/\sigma > 0.08$. With the dynamic inflow model, the minimum damping level for $0.01 \leq C_T/\sigma \leq 0.02$ is well predicted. Although all three analyses predict increases in damping at negative thrust conditions, insufficient experimental data exist to verify this trend. A greater influence of dynamic inflow would be expected if the rotor installation allowed significant shaft motions (ground resonance or air resonance behavior).

The influence of the cyclic rotor control-system mode on predicted damping levels at a rotor rotational speed of 425 rpm is shown in Figure 13. A dynamic inflow model is used for the analysis. Nonrotating frequencies (per rev) between $6.3 \leq \omega_\theta \leq 9.3$ are shown. The corresponding rotor cyclic control-system stiffness is given in Table 4. In Table 4, the calculated first elastic torsion mode frequency does not vary as a function of cyclic control-system stiffness. This shows that it is a cyclic control-system stiffness variation and not a variation of the torsional stiffness. The baseline value used in obtaining the results shown in Figures 11 and 12 is $\omega_\theta = 7.3$ per rev. Although the cyclic control-system stiffness has only moderate influence in reducing damping at high thrust levels, increasing the stiffness can increase the damping at low thrust levels (over 23% for the minimum damping value at $C_T/\sigma = 0.02$). Because of the lack of experimental data for the wind tunnel test configuration, a value of $\omega_\theta = 7.3$ per rev was selected as the baseline value for the results presented in this paper. This results in a rotor test apparatus control-system stiffness that is approximately the same as that of the rotor when it is installed on a BO-105 flight aircraft; the stiffness is also equal to that of other similar rotor control-systems previously tested on the Ames Rotor Test Apparatus.

FORWARD FLIGHT RESULTS

Forward flight predictions of the BO-105 rotor system on the Ames Rotor Test Apparatus for 1-g thrust conditions at advance ratios of 0.0 to 0.35 are presented in Figures 14-16. The results presented here support the pretest predictions for a future BO-105 rotor test on the Ames Rotor Test Apparatus in the NASA Ames 40- by 80-Foot Wind Tunnel. The influence of different aerodynamic inflow models, dynamic inflow models, and shaft angle variations on predicted stability levels are shown as a function of advance ratio, μ. Two bending and two torsion rotor modes were used in the aeroelastic stability analysis for all results presented since additional rotor modes did not influence the predicted results. The effect of using from zero to seven support degrees of freedom in the analysis on the predicted damping was briefly investigated. Although not presented in this paper, the results demonstrated that the support degrees of freedom did not significantly influence the predicted damping of the inplane modes. A free wake analysis was used for all forward flight predictions presented in this paper.

The influence of different aerodynamic inflow models on the predicted regressing inplane damping as a function of advance ratio is presented in Figure 14. Results presented are for a simulated 1-g thrust condition ($C_T/\sigma = 0.07$) and a constant propulsive force as trimmed in the wind tunnel environment. The analysis trimmed to a rotor drag force of 16.5 ft^2 by varying rotor shaft angle in addition to trimming collective and cyclic pitch for thrust in the trim solution. Results are shown for a constant rotor rotational speed of 425 rpm with a static aerodynamic inflow model, a quasi-static inflow model, and a dynamic inflow model. All three inflow models predict a minimum damping level at an advance ratio of about 0.15, which is consistent with the flight test results presented in Refs. 6 and 7. The static inflow model predicts the least amount of damping, while the quasi-static inflow model predicts the highest level of damping at an advance ratio of 0.15. For consistency with the hover results, the dynamic inflow model is used for the remaining results presented in this paper.

The influence of different dynamic inflow models used in the aeroelastic stability analysis on the predicted regressing inplane damping as a function of advance ratio is presented in Figure 15. Two dynamic inflow models are compared as a function of advance ratio (0.0 to 0.35) at a constant 1-g rotor thrust ($C_T/\sigma = 0.07$) and constant propulsive force. The Pitt and Peters dynamic inflow model[11] is compared to a perturbation form of the empirical inflow model.[2] The Pitt and Peters model uniformly predicts less damping for advance ratios from 0.15 to 0.30. In hover and at an advance ratio of 0.35 there are no significant differences between the two models. Again, more influence of dynamic inflow is expected with shaft motions involved.

The influence of shaft angle on the predicted regressing inplane damping as a function of advance ratio are presented in Figure 16. Typical wind tunnel testing consists of varying rotor thrust and advance ratio at fixed rotor shaft angles to maximize the number of test conditions at which data are acquired. Results for three shaft angles are presented and compared with the dynamic inflow results presented in Figure 14. As in Figure 14, results are presented as a function of advance ratio at a constant 1-g rotor thrust ($C_T/\sigma = 0.07$). At a shaft angle of $-5°$, the regressing inplane damping results are insensitive to advance ratio. As the rotor shaft angle is decreased ($-5°$ to $-10°$, and $-10°$ to $-15°$) the regressing inplane damping increases for all advance ratios presented.

CONCLUSIONS

A full-scale BO-105 hingeless helicopter rotor system was tested in hover. The rotor system structural model was validated with

blade bending and torsional moment data. Damping of the regressing inplane rotor mode was determined for trends with changing rotor thrust and tip speed. An improved data reduction technique was used to determine the aeroelastic stability from existing transient decay records. Experimental data have been compared with analytical predictions. Forward flight predictions, in support of future testing of the BO-105 rotor system on the Ames Rotor Test Apparatus for 1-g thrust conditions at advance ratios of 0.0 to 0.35 are presented. The major findings of this study are as follows:

1. BO-105 rotor system blade bending (flapwise and edgewise) and torsional moment trends and magnitudes are well predicted as a function of rotor thrust at a constant rotational speed of 425 rpm. An aft shift in the elastic axis location from 15.6% chord to 17.95% chord (0.25 inches aft), results in improved correlation of the edgewise bending moment predictions with experimental data.

2. BO-105 rotor system damping varies with rotor thrust at a constant rotational speed of 425 rpm. A minimum damping level is obtained at a C_T/σ of about 0.02.

3. Damping trends are well predicted with a comprehensive state-of-the-art rotorcraft analysis. Although the predicted results were insensitive to the number of support-system modes modeled, the first two elastic bending modes and the first rigid and elastic torsion modes of the blades were required for adequate correlation.

4. Neither minimum damping levels nor damping trends with thrust at constant rotation speed for the regressing inplane mode are accurately predicted using a quasi-static inflow model. The minimum damping level is well predicted using a static inflow model. Damping predictions are improved at low thrust conditions ($C_T/\sigma \leq 0.04$) using a dynamic inflow model.

5. Damping trends as a function of advance ratio at 1-g thrust conditions ($C_T/\sigma = 0.07$) compare well with published flight test results. Minimum damping as a function of advance ratio are predicted by all three aerodynamic inflow models.

6. The damping level of the regressing inplane mode is relatively insensitive at advance ratios below 0.25. As rotor shaft angle decreases (nose-down) from $-5°$ to $-15°$, damping increases for all advance ratios, particularly at the higher speeds.

REFERENCES

[1]Peterson, R. L. and Warmbrodt, W., "Hover Test of a Full-Scale Hingeless Helicopter Rotor: Aeroelastic Stability, Performance and Loads Data," NASA TM-85892, Jan. 1984.

[2]Johnson, W., "A Comprehensive Analytical Model of Rotorcraft Aerodynamics and Dynamics, Theory Manual, Johnson Aeronautics Version," Johnson Aeronautics, 1989.

[3]Peterson, R. L. and Warmbrodt, W., "Hover Performance and Dynamics of a Full-Scale Hingeless Rotor," *Journal of the American Helicopter Society*, Vol. 31, No. 3, July 1986.

[4]Peterson, R. L., Warmbrodt, W., and Hoover, J., "Aeromechanical Stability of a Full-Scale Hingeless Rotor in Hover," *Proceedings of the 40th Annual Forum of the American Helicopter Society*, Arlington, VA, May 1984.

[5]Staley, J. A., "Validation of Rotorcraft Flight Simulation Program through Correlation with Flight Data for Soft In-Plane Hingeless Rotors," USAAMRDL TR-75-50, Jan. 1976.

[6]Kloppel, V., Kampa, K., and Isselhorst, B., "Aeromechanical Aspects in the Design of Hingeless/Bearingless Rotor Systems," *Proceedings of the Ninth European Rotorcraft Forum*, Stressa, Italy, Sept. 1983.

[7]Huber, H. B., "Effect of Torsional-Flap-Lag Coupling on Hingeless Rotor Stability," *Proceedings of the 29th Annual Forum of the American Helicopter Society*, Washington, D.C., May 1973.

[8]Hammond, C. E. and Doggett, R., "Demonstration of Subcritical Damping by Moving Block/Randomdec Applications," NASA SP-415, 1976, pp.59-76.

[9]Wilcox, P. R. and Crawford, W. L., "A Least Squares Method For The Reduction Of Free Oscillation Data," NASA TN D-4503, June 1968.

[10]Braun, D. and Huber, H., "Design and Development Tests of a Five-Bladed Hingeless Helicopter Main Rotor," *Proceedings of the Fourteenth European Rotorcraft Forum*, Milano, Italy, Sept. 1988.

[11]Gaonkar, G. H. and Peters, D. A., "Review of Dynamic Inflow Modelling for Rotorcraft Flight Dynamics," AIAA Paper No. 86-0845, May 1986.

ITEM	SPECIFICATION
Type	Hingeless
Radius (ft)	16.11
Number of blades	4
Blade chord (ft)	0.866
Linear blade twist (deg)	-8
Precone (deg)	$2.5°$
Solidity, σ	0.07
Reference area, S (ft^2)	5.30
Airfoil section	NACA 23012

TABLE 1. BO-105 MAIN ROTOR DATA

	FIRST MODE	SECOND MODE	THIRD MODE
Flapwise	1.12	2.78	5.02
Edgewise	0.66	4.33	11.20
Torsion	3.79	10.53	17.32

TABLE 2. CALCULATED ROTATING BLADE FREQUENCIES (PER REV) AT 425 RPM, COLLECTIVE PITCH = 9.7°

	CHORD LOCATION (% AFT OF LEADING EDGE)
Elastic Axis	15.6
Feathering Axis	15.6
Tension Axis	21.1
C. G. Axis	24.4
Control Axis	25.0

TABLE 3. BASELINE ROTOR BLADE CROSS-SECTIONAL STRUCTURAL MODELING PARAMETERS.

ω_θ 1/rev	ω_θ rad/sec	k_θ ft-lb/rad	FIRST ELASTIC TORSION MODE FREQUENCY
6.3	280.4	6,120	3.79
7.3	324.9	8,220	3.79
8.3	369.4	10,630	3.79
9.3	413.9	13,340	3.79

TABLE 4. CONTROL-SYSTEM STIFFNESS VARIATIONS USED IN FIGURE 13: 425 RPM, I_θ = 0.0795 SLUG-FT^2.

FIGURE 2. BO-105 HINGELESS ROTOR HUB.
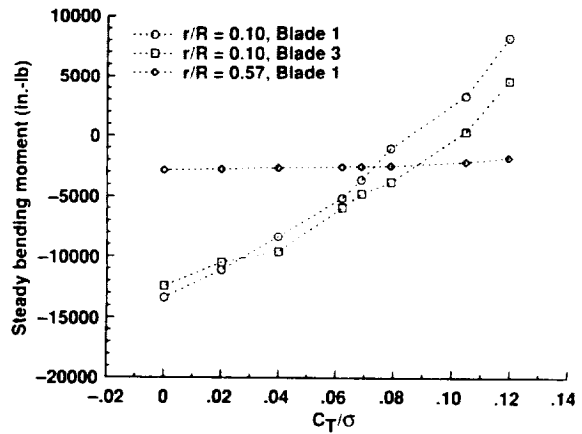
FIGURE 3. EXPERIMENTAL EDGEWISE BENDING MOMENT DATA, 425 RPM.

FIGURE 1. BO-105 ROTOR SYSTEM ON AMES ROTOR TEST APPARATUS IN 40- BY 80-FOOT WIND TUNNEL TEST SECTION.
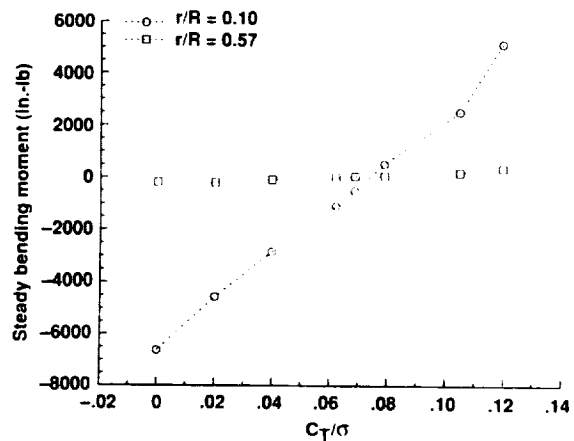
FIGURE 4. EXPERIMENTAL FLAPWISE BENDING MOMENT DATA, 425 RPM.
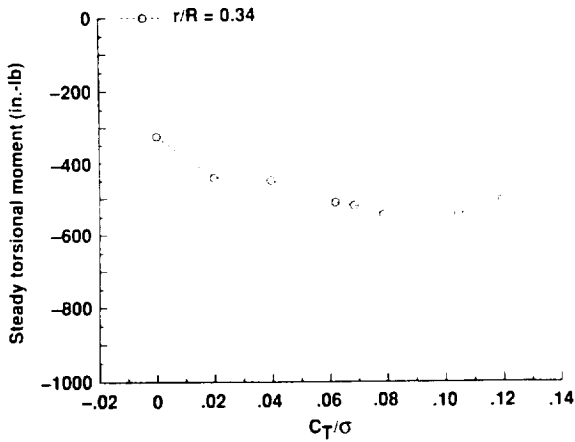
FIGURE 5. EXPERIMENTAL TORSIONAL MOMENT
DATA, 425 RPM.
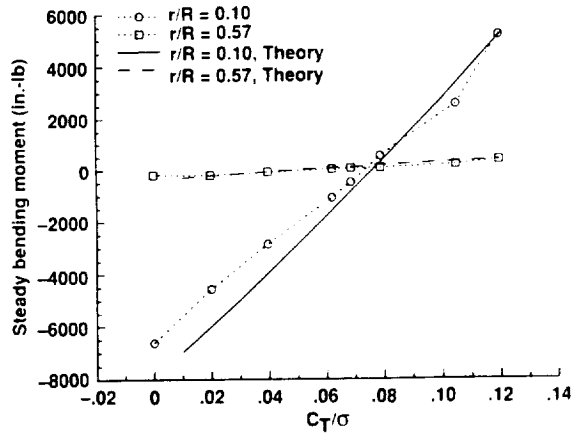
FIGURE 8. CORRELATION OF FLAPWISE BENDING
MOMENT DATA WITH ANALYTICAL RESULTS, 425 RPM.
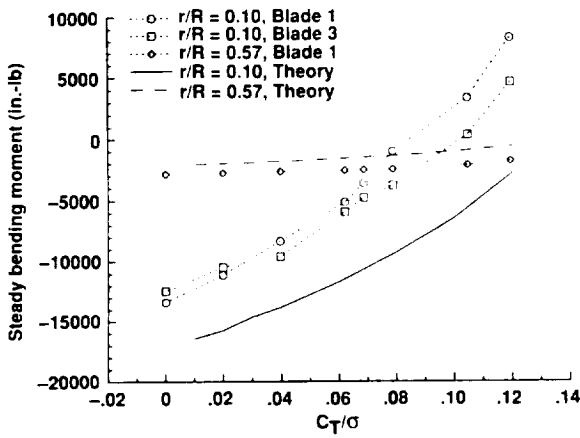
FIGURE 6. CORRELATION OF EDGEWISE BENDING
MOMENT DATA WITH ANALYTICAL RESULTS, 425 RPM.
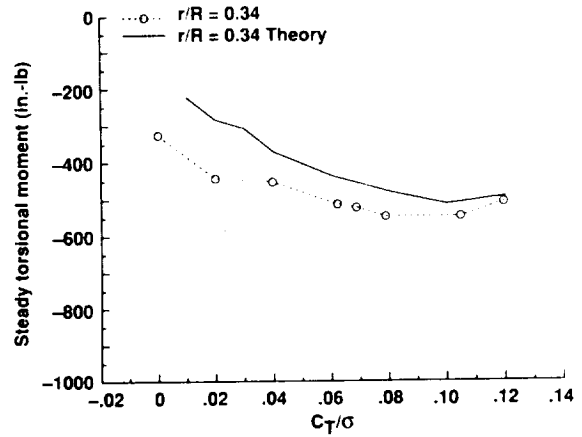
FIGURE 9. CORRELATION OF TORSIONAL MOMENT
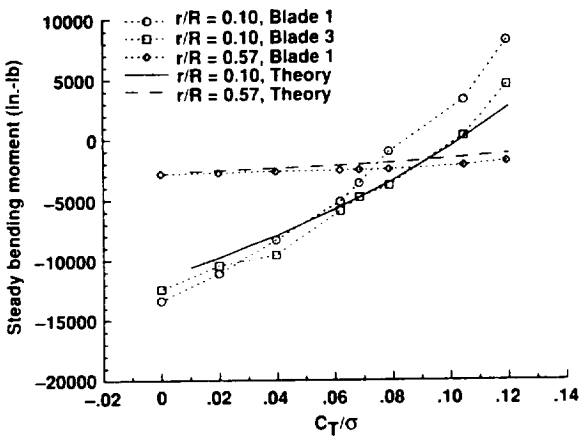DATA WITH ANALYTICAL RESULTS, 425 RPM.

FIGURE 7. CORRELATION OF EDGEWISE BENDING
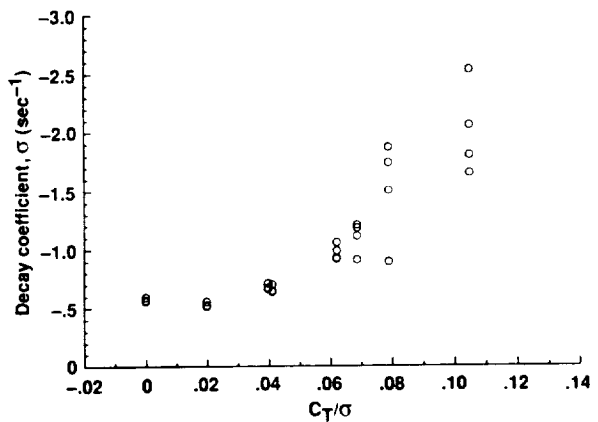MOMENT DATA WITH REVISED ELASTIC AXIS LOCA-
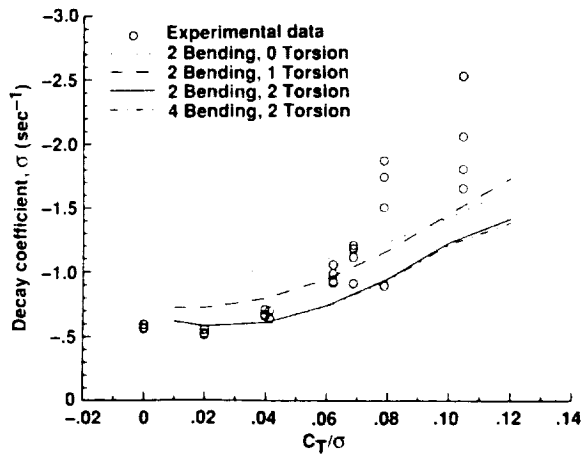TION, 425 RPM.

FIGURE 10. ROTOR REGRESSING INPLANE MODAL
DAMPING, 425 RPM.

FIGURE 11. EFFECT OF NUMBER OF ROTOR BLADE MODES ON PREDICTED DAMPING LEVELS, 425 RPM.
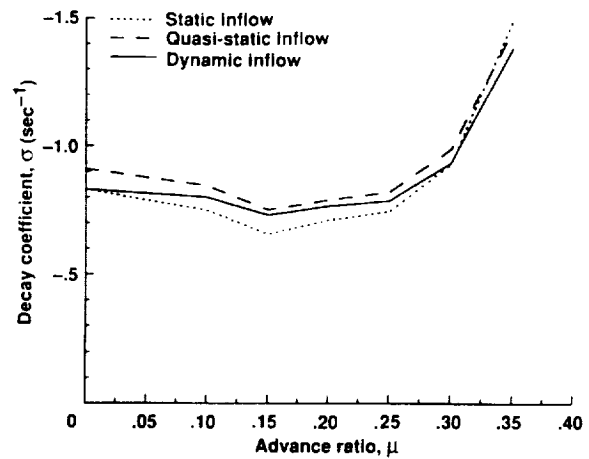
FIGURE 14. EFFECT OF DIFFERENT AERODYNAMIC INFLOW MODELS ON PREDICTED DAMPING LEVELS, 425 RPM, $C_T/\sigma = 0.07$.
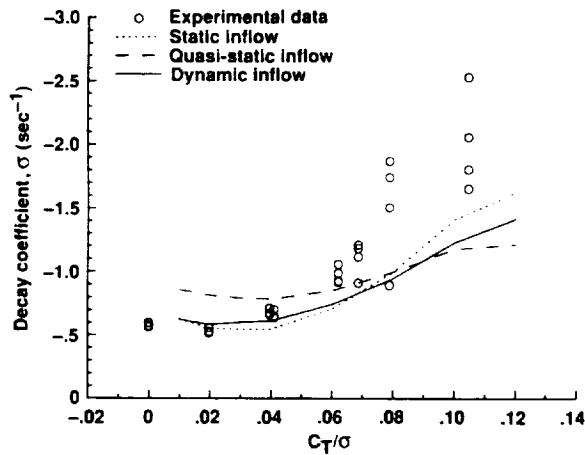
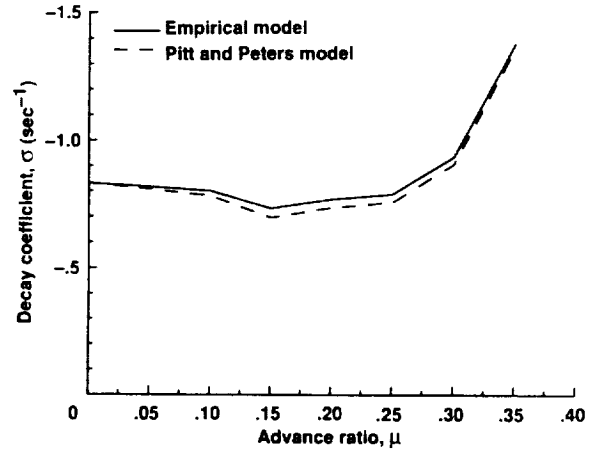FIGURE 12. EFFECT OF DIFFERENT AERODYNAMIC INFLOW MODELS ON PREDICTED DAMPING LEVELS, 425 RPM.

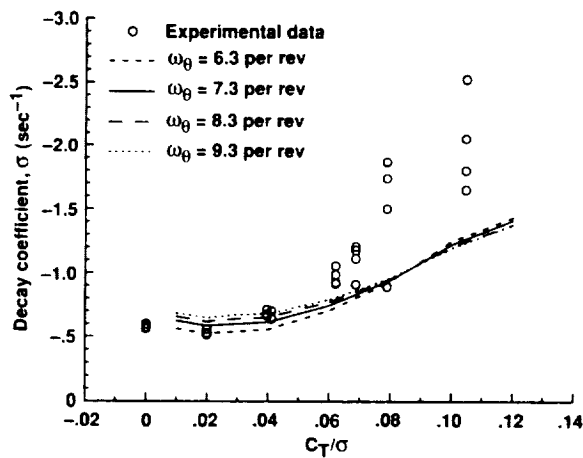FIGURE 15. EFFECT OF DYNAMIC INFLOW MODELS ON PREDICTED DAMPING LEVELS, 425 RPM, $C_T/\sigma = 0.07$.

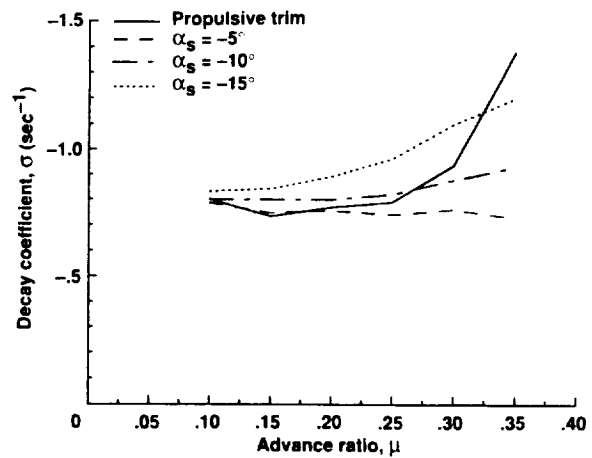FIGURE 13. EFFECT OF ROTOR CYCLIC CONTROL-SYSTEM FREQUENCY ON PREDICTED DAMPING LEVELS, 425 RPM.

FIGURE 16. EFFECT OF ROTOR SHAFT ANGLE ON PREDICTED DAMPING LEVELS, 425 RPM, $C_T/\sigma = 0.07$.

8

REPORT DOCUMENTATION PAGE

Public reporting burden for this collection of information is estimated to average 1 hour per response, including the time for reviewing instructions, searching existing data sources, gathering and maintaining the data needed, and completing and reviewing the collection of information. Send comments regarding this burden estimate or any other aspect of this collection of information, including suggestions for reducing this burden, to Washington Headquarters Services, Directorate for Information Operations and Reports, 1215 Jefferson Davis Highway, Suite 1204, Arlington, VA 22202-4302, and to the Office of Management and Budget, Paperwork Reduction Project (0704-0188), Washington, DC 20503.

1. AGENCY USE ONLY *(Leave blank)*	2. REPORT DATE July 1991	3. REPORT TYPE AND DATES COVERED Technical Memorandum-Final

4. TITLE AND SUBTITLE

Aeroelastic Loads and Stability Investigation of a Full-Scale Hingeless Rotor

5. FUNDING NUMBERS

505-59-36

6. AUTHOR(S)

Randall L. Peterson and Wayne Johnson (Johnson Aeronautics, Palo Alto, CA)

7. PERFORMING ORGANIZATION NAME(S) AND ADDRESS(ES)

Ames Research Center
Moffett Field, CA 94035-1000

8. PERFORMING ORGANIZATION REPORT NUMBER

A-91157

9. SPONSORING/MONITORING AGENCY NAME(S) AND ADDRESS(ES)

National Aeronautics and Space Administration
Washington, DC 20546-0001

10. SPONSORING/MONITORING AGENCY REPORT NUMBER

NASA TM-103867

11. SUPPLEMENTARY NOTES

12a. DISTRIBUTION/AVAILABILITY STATEMENT

Unclassified-Unlimited
Subject Category – 05

12b. DISTRIBUTION CODE

13. ABSTRACT *(Maximum 200 words)*

An analytical investigation was conducted to study the influence of various parameters on predicting the aeroelastic loads and stability of a full-scale hingeless rotor in hover and forward flight. The CAMRAD/JA (for Comprehensive Analytical Model of Rotorcraft Aerodynamics and Dynamics, Johnson Aeronautics) analysis code is used to obtain the analytical predictions. Data are presented for rotor blade bending and torsional moments as well as inplane damping data obtained for rotor operation in hover at a constant rotor rotational speed of 425 rpm and thrust coefficients between 0.0 and 0.12. Experimental data presented are from a test in the NASA Ames 40- by 80-Foot Wind Tunnel. Validation of the rotor system structural model with experimental rotor blade loads data shows excellent correlation with analytical results. Using this analysis, the influence of different aerodynamic inflow models, the number of generalized blade and body degrees of freedom, and the control-system stiffness at predicted stability levels are shown. Forward flight predictions of the BO-105 rotor system on the Ames Rotor Test Apparatus for 1-g thrust conditions at advance ratios of 0.0 to 0.35 are presented. The influence of different aerodynamic inflow models, dynamic inflow models and shaft angle variations on predicted stability levels are shown as a function of advance ratio.

14. SUBJECT TERMS

Helicopters, Rotary wing, Rotor aerodynamics, Aeroelastic stability, Rotor loads

15. NUMBER OF PAGES

9

16. PRICE CODE

A02

17. SECURITY CLASSIFICATION OF REPORT	18. SECURITY CLASSIFICATION OF THIS PAGE	19. SECURITY CLASSIFICATION OF ABSTRACT	20. LIMITATION OF ABSTRACT
Unclassified	Unclassified		